ON THE X-RAY OUTBURST LIGHT CURVES AND RECURRENCE CHARACTERISTICS OF X-RAY TRANSIENTS WITH NEUTRON STARS

by
ÖMER FARUK ÇOBAN

Submitted to the Graduate School of Engineering and Natural Sciences
in partial fulfilment of
the requirements for the degree of Master of Science

Sabancı University
December 2022

ON THE X-RAY OUTBURST LIGHT CURVES AND RECURRENCE CHARACTERISTICS OF X-RAY TRANSIENTS WITH NEUTRON STARS

Approved by:

Prof. ÜNAL ERTAN .....
(Thesis Supervisor)

Asst. Prof. AYŞE ULUBAY .....

Prof. EMRAH KALEMCİ .....

Date of Approval: Dec 27, 2022

ABSTRACT

ON THE X-RAY OUTBURST LIGHT CURVES AND
RECURRENCE CHARACTERISTICS OF
X-RAY TRANSIENTS WITH NEUTRON STARS

ÖMER FARUK ÇOBAN

Physics M.Sc. Thesis, Dec 2022

Thesis Supervisor: Prof. Ünal Ertan

Keywords: accretion, accretion discs, binaries, Aql X-1, instabilities

It was proposed earlier that the knee-like morphology followed by a sharp decay in the outburst light curves of some magnetised stars, including the prototypical neutron star X-ray transient (NSXT) Aql X-1, could be an indication of the transition to the propeller phase. In this thesis, we first investigate the effects of the disc parameters, namely the X-ray irradiation strength, the kinematic viscosity, the initial mass distribution, and the disc mass on the decay characteristics of the X-ray outburst light curves of NSXTs in the frame of the disc instability model. Our results show that the typical features of the outburst light curves of Aql X-1 cannot be obtained by simply changing one or some of these parameters. Subsequently, with detailed numerical analysis, we have shown that the entire X-ray outburst light curve can be reproduced by taking the weak disc mass flow rate dependence of the disc aspect ratio and its effect on the X-ray irradiation strength into account in the calculations. When the mass flow from the companion into the outer disc is included in the calculations, the same model can also yield recurrent outbursts with morphology and recurrence times similar to those observed from Aql X-1. In our model, the X-ray light curve of the source is produced by mass accretion onto the neutron star throughout the outburst phase without including any propeller effect or partial accretion regime, as proposed in earlier work to explain the decay features of the outburst light curve of Aql X-1.

ÖZET

GEÇİCİ X-IŞINI NÖTRON YILDIZLARININ X-IŞIMASI PARLAMA IŞIK EĞRİLERİ VE YİNELENME KARAKTERİSTİKLERİ ÜZERİNE

ÖMER FARUK ÇOBAN

Fizik Yüksek Lisans Tezi, Aralık 2022

Tez Danışmanı: Prof. Dr. Ünal Ertan

Anahtar Kelimeler: kütle aktarım, kütle aktarım diskleri, çift sistemler, Aql X-1, kararsızlıklar

Prototipik geçici X-ışını nötron yıldızı (NSXT) Aql X-1'in de içlerinde bulunduğu bazı manyetik yıldızların parlama ışık eğrilerindeki diz benzeri morfolojinin ve devamındaki keskin düşüşün pervane fazına geçişin belirtisi olduğu öne sürülmüştür. Bu tezde, ilk olarak X-ışını ısıtma gücü, kinematik viskozite, başlangıç kütle dağılımı ve disk kütlesi gibi disk parametrelerin, NSXT'lerin X-ışını parlama ışık eğrilerindeki düşüşe etkilerini disk kararsızlık modeli çerçevesinde araştırdık. Sonuçlarımız, Aql X-1'in parlama ışık eğrilerinin tipik özelliklerinin, bu parametrelerden birini veya birkaçını değiştirerek elde edilemeyeceğini göstermektedir. Daha sonra, detaylı sayısal hesaplamalarla, tüm X-ışını parlama ışık eğrisinin, disk kalınlık geometrisinin kütle-akış miktarına olan zayıf bağımlılığı ve bunun X-ışını ısıtma gücüne etkisi hesaba katıldığında üretilebildiğini gösterdik. Aynı model, eş yıldızdan dış diske kütle aktarımı da hesaplamalara dahil edildiğinde, Aql X-1'den gözlemlenenlere benzer morfolojide ve tekrarlama sıklığında tekrarlanan parlamaları da üretebilmektedir. Modelimizde, parlama fazı boyunca gözlemlenen X-ışını ışıma gücünü, pervane fazı ve daha önceki çalışmalarda Aql X-1'in parlama ışık eğrilerinin düşüş fazı özelliklerini açıklamak için önerilmiş bir kısmi kütle aktarım rejimine gerek kalmaksızın, nötron yıldızına devamlı kütle aktarımıyla üretebilmekteyiz.

ACKNOWLEDGEMENTS

I would like to express my deepest gratitude to my supervisor, Prof. Ünal Ertan, for his constant support and guidance throughout my graduate studies. His knowledge, insights, and encouragement have been invaluable in my growth as a researcher and scholar. I am deeply grateful for his endless patience and faith in me and my abilities. I would also like to thank the jury members, Asst. Prof. Ayşe Ulubay and Prof. Emrah Kalemci, as well as Prof. M. Ali Alpar, for their valuable comments and suggestions.

Additionally, I want to express my gratitude to Ali Arda Gençali, a friend and supporter who has spent countless hours with me in discussion and brainstorming. I also like to express my gratitude to my friend, Dr. Ali Murtaza Altıngün, for his encouragement and support during my graduate studies.

Finally, I am deeply grateful to all the individuals whose names are not mentioned here for their fellowship in my graduate journey.

I acknowledge research support from TÜBİTAK (The Scientific and Technological Research Council of Turkey) through grant 120F329 and the full scholarship from the faculty of engineering and natural sciences of Sabancı University.

TABLE OF CONTENTS

LIST OF FIGURES ..... **viii**

LIST OF ABBREVIATONS ..... **x**

1. INTRODUCTION **1**

2. DISC INSTABILITY MODEL **5**

3. APPLICATION TO AQL X-1 ..... **7**

3.1. Introduction 7

3.2. Model 10

3.3. Parameter Study 13

3.4. Results and Discussion 21

3.4.1. The 2010 Outburst of Aql X-1 21

3.4.2. The Quiescent State and Recurrent Outbursts 22

4. SUMMARY AND CONCLUSIONS **25**

BIBLIOGRAPHY **28**

LIST OF FIGURES

Figure 2.1. Temperature - Surface density diagram (S-Curve) 6

Figure 3.1. The X-ray outburst light curve produced by simulation 1 (top panel). The bottom panel shows the variation of $r_{\rm h}$ during the outburst. The model parameters are: $\alpha_{\rm h} = 0.1$, $\alpha_{\rm c} = 0.01$, $C = 2 \times 10^{-4}$ and $M_{\rm disc} = 2 \times 10^{24}$ g..... 14

Figure 3.2. Model curves for different initial mass distributions. Δr and Σ_0 values are given in the figure. The initial disc mass $M_{\rm disc} = 2 \times 10^{24}$ g is the same for the three illustrative models. The dotted line is the model curve obtained in simulation 1 Fig. (3.1)..... 15

Figure 3.3. Illustrative model curves for different disc masses. The blue and green solid lines are obtained with $M_{\rm disc} = 6 \times 10^{24}$ g and $M_{\rm disc} = 6.7 \times 10^{23}$ g, respectively. The dotted line is the model curve obtained in the first simulation. 16

Figure 3.4. Model curves for different $\alpha_{\rm h}$ parameters. The blue and green solid lines represent the results with $\alpha_{\rm h} = 0.15$ and $\alpha_{\rm h} = 0.08$, respectively. The dotted line shows the model curve obtained in Fig. (3.1). . 17

Figure 3.5. Model curves for different $\alpha_{\rm c}$ parameters. The solid blue line is produced with $\alpha_{\rm c} = 5 \times 10^{-3}$. The dotted line shows the model curve obtained in simulation 1 with $\alpha_{\rm c} = 1 \times 10^{-2}$ (Fig. 3.1). 18

Figure 3.6. Model curves for different irradiation strengths. We obtain the solid and dotted lines with $C = 4 \times 10^{-4}$ and $C = 2 \times 10^{-4}$, respectively. The dotted line shows the model curve obtained in reference simulation 1 (Fig. 3.1). 19

Figure 3.7. X-ray irradiation with variable and constant h/r. In the top panel, solid and dotted lines show the model light curves produced by $\dot{M}$ dependent and constant irradiation parameters (see Sec. 3.2). The curves in the bottom panel show the $r_{\rm h}$ evolution during the outburst. 20

Figure 3.8. X-ray outburst light curve of Aql X-1 (taken from Campana et al. (2014)). The solid model curve is obtained with $\alpha_{\rm c} = 5 \times 10^{-3}, \alpha_{\rm h} = 0.1, \mu_{\rm c} = 0.9, \mu_{\rm h} = 0.6$, and $C_0 = 1.3 \times 10^{-4}$. For the $L_{\rm X}$ calculation, we take $\dot{M}_* = \dot{M}_{\rm in}$ for the entire model curve. 22
Figure 3.9. The same model parameters are used for the solid curve in Fig. (3.8). This model curve is obtained by injecting mass into the radial grid at $r = r_{\rm circ}$ with a rate of 4×10^{16} g s^{-1}. The recurrence time of the outbursts is approximately one year. The second outburst seen in this figure is enlarged in Fig. (3.10) 24
Figure 3.10. The second outburst seen in Fig. (3.9)..... 24

LIST OF ABBREVIATONS

BH Black Hole 1, 2, 6, 7

BHXT Black Hole X-ray Transient 6, 7, 8, 10

DIM Disc Instability Model 6, 8, 9, 25, 26

DN Dwarf Nova 5, 6, 8, 9

EM Electromagnetic 1, 2

FRED Fast Rise Exponential Decay 10

HMXB High-Mass X-ray Binary 2

INTEGRAL International Gamma-Ray Astrophysics Laboratory 2

LMXB Low-Mass X-ray Binary 2, 3, 7, 8, 9, 11, 13

NS Neutron Star 1, 2, 6, 7, 11, 12, 13, 14

NSXT Neutron Star X-ray Transient 3, 6, 7, 8, 9, 25

RXTE Rossi X-ray Timing Explorer 2

tMSP transitional Millisecond Pulsar 13, 23

1. INTRODUCTION

In the late evolutionary phases of a massive star ($M > 8M_{\odot}$), thermo-nuclear reactions terminate at the core, and thermal pressure becomes insufficient to support the star against gravity. Then, the star collapses in a short time, ejecting its outer layers with an immense explosion, a "supernova", which may produce either a neutron star (NS) or a black hole (BH) depending on the mass of the progenitor star. During the collapse of the core of the star, electrons become degenerate. Unlike low-mass stars, electron degeneracy pressure cannot prevent the collapse of high-mass stars. Under extreme densities, electrons and protons combine to form neutrons (Baade & Zwicky, 1934). If the neutron degeneracy pressure can prevent further collapse, the core becomes a NS with a radius of $R \simeq 10^6$ cm and a mass of $M \sim 1M_{\odot}$, where $M_{\odot} = 1.99 \times 10^{33}$ g is the solar mass. For sufficiently high progenitor masses ($\gtrsim 25M_{\odot}$), even neutron degeneracy pressure cannot stop the collapse, and the core becomes a BH. Due to the conservation of angular momentum during the core collapse, newly formed NS rotates rapidly with a period, P, of the order of milliseconds. Similarly, due to magnetic flux conservation during the collapse, young NSs are born with very strong magnetic dipole fields with a strength of $\sim 10^{12}$ G on the surface.

With these extreme dipole fields and high rotation rates, NSs emit strong magnetic dipole radiation observed in different wavelengths of the electromagnetic (EM) spectrum. The closed magnetic field lines co-rotate with the NS. Since the speed of the field lines cannot exceed the speed of light, the field lines are open outside the so-called light cylinder radius $r_{\rm LC} = c/\Omega_*$, where c is the speed of light, and Ω_* is the rotational angular speed of the star. The charged particles are accelerated along the open field lines emerging from the poles of the star and produce synchrotron radiation near the poles. Since magnetic field lines are nearly parallel close to the magnetic poles, accelerated charged particles emit radio waves propagating in a narrow cone. The magnetic and rotational axes of these stars are usually not aligned. As the NS rotates, the radio beam sweeps a portion of the sky. If the earth is in this portion of the sky, the radiation from the source seems like turning on and off with a period equal to the spin period of the star. These NSs are called "pulsars".

In 1968, Gold (1968) proposed that NSs lose their rotational energies through magnetic field dipole radiation. Eventually, their rotational powers decrease below a threshold and become insufficient to produce pulsed radio emission. Up to now, nearly 2600 radio pulsars have been detected (Manchester et al., 2005). Rotational periods of radio pulsars range from as short as 1.4 ms (Hessels et al., 2006) to long periods such as 23.5 s (Tan et al., 2018) with period derivatives $\dot{P}$ ranging from approximately 10^{-20} s s^{-1} to 10^{-12} s s^{-1}. Many radio pulsars also emit pulsed radiation from optical to gamma-ray bands of the EM spectrum along with radio pulses.

There are many NSs in binary systems as well. Depending on the companion mass, $M_{\rm c}$, they are classified as high-mass X-ray binaries (HMXBs; $M_{\rm c} > 10 M_{\odot}$) or low-mass X-ray binaries (LMXBs; $M_{\rm c} < 1 M_{\odot}$). In these systems, mass flow from the companion onto the compact star is a very efficient high-energy radiation mechanism. NSs and BHs could accrete matter from their companions in close binary systems. There are two possible mechanisms of mass transfer from the companion onto the compact star:

- During some phases of evolution, the companion may eject a great part of its mass with stellar winds; a fraction of this material is captured by the compact star. Mass transfer via this process is called stellar wind accretion.
- During its evolution, the companion expands on its way to becoming a red giant, or the binary separation decreases sufficiently for the gravitational field of the compact star to tear away the outer layers of the gas companion. Mass transfer via this process is called Roche lobe overflow.

The stellar wind accretion is mainly observed in HMXBs. In these systems, companion stars are either main-sequence Be stars or supergiants of the O/B types. Be stars are surrounded by an ejected circumstellar gas disc, and every time the compact star passes through the disc, disc matter flowing onto the star produces hard X-ray radiation. In HMXBs with supergiant companions, accretion occurs due to stellar wind resulting from high radiation pressure. In such systems, part of the wind matter is captured by the gravitational field of the compact star and flows onto the star. Since the lifetimes of massive stars are very short, these binaries cannot migrate far from their birth location. Hence, HMXBs are located in the star-forming regions of the galactic plane. So far, around 200 HMXBs are detected (Kretschmar et al., 2019; Liu et al., 2006) by the observations of Rossi X-ray Timing Explorer (RXTE) and International Gamma-Ray Astrophysics Laboratory (INTEGRAL).

In most LMXBs, the compact star accretes matter from the companion through

the Roche lobe overflow mechanism. In these systems, the companion star could be a main-sequence star, an F-G type subgiant, a white dwarf, or an A-type star (Sazonov et al., 2020). In LMXBs, the low-mass companion expands and fills its Roche lobe, and the matter from the outer layers of the star starts to flow into the Roche lobe of the compact object through the first Lagrangian (L_1) point. Due to its initial angular momentum, matter spirals into an eccentric orbit around the compact star instead of falling directly onto the star (Frank et al., 2002). Matter continuously flowing through the L_1 point interacts with matter flowing into the same orbit, resulting in energy dissipation with shocks. The matter then settles into a circular orbit around the star, the lowest energy orbit for a given angular momentum. The radius of this circular orbit is called circularisation radius, $r_{\rm circ}$. As a result of continuous mass flow from the companion, the matter that piles up at $r_{\rm circ}$ spreads to both outer and inner radii through viscous processes forming an accretion disc around the compact star. While dissipating part of the kinetic energies, viscous interactions also redistribute the angular momentum during and after the disc formation.

Persistent LMXBs are luminous X-ray sources with roughly constant accretion luminosities ($L_{\rm X} \sim 10^{36} - 10^{38}$ erg s^{-1}). A large fraction of LMXBs are transient systems that show repetitive X-ray outbursts with varying recurrence times, durations and $L_{\rm X}$ peaks. Our work in this thesis is on the X-ray light curves of transient LMXBs containing neutron stars (NSXTs). Most of the time, these systems remain in their quiescence states with low $L_{\rm X} \sim 10^{32} - 10^{34}$ erg s^{-1} that last for years and occasionally months. Their outburst states last from weeks to months (they can rarely last for years). During an outburst, the $L_{\rm X}$ of the source increases by several orders of magnitude (up to $\sim 10^{38}$ erg s^{-1}) within a few days. The X-ray outbursts last $\sim$ 10 to 100 days, and sources return back to quiescence with roughly exponential decay. This transient nature of LMXBs is likely to be resulting from instabilities in accretion discs (see Ch. 2). Due to their low $L_{\rm X}$ in the quiescent state, transient LMXBs are usually discovered in their outburst states by all-sky survey telescopes with a wide field of view.

Among these NSXTs, Aql X-1, with very well-known outburst properties, provides an excellent laboratory to study the physics of accretion disc in LMXBs. Some features observed during the outburst decay phase of this source were proposed to be a sign of its transition into the propeller phase (Campana et al., 2014). In this thesis, we will concentrate on the characteristic features of the X-ray outburst light curves of Aql X-1. In the frame of the disc instability model, we will try to model the outburst light curve of the source and investigate whether the onset of the propeller effect or varying partial accretion, as proposed earlier (Lipunova et al., 2022) are

indeed required to reproduce the observed X-ray outburst light curves.

In Chapter 2, we describe the disc instability model. The details of the numerical code used in this thesis with a parameter study for the application of our model to the 2010 outburst light curve and recurrence properties of Aql X-1 are given in Chapter 3. We summarise our results and conclusions in Chapter 4.

2. DISC INSTABILITY MODEL

The accretion disc instabilities were first proposed by Smak (1971) and Osaki (1974) to explain the outbursts of dwarf novae (DNs), a subclass of catalytic variables. DNs are binary systems in which a K-type or an M-type companion star transfers matter via Roche lobe overflow onto a white dwarf. DNs show quasi-periodic outbursts with short time-scales (weeks to months). To explain these outbursts, Smak (1971) and Osaki (1974) proposed an unspecified mechanism that causes matter to accumulate in the disc during the quiescence phase, and the accumulated matter flows onto the white dwarf in a very short time, producing an outburst. A physical mechanism was proposed by Hōshi (1979) about five years later. Hoshi obtained equilibrium solutions relating the effective temperature, $T_{\rm eff}$, to disc surface density, Σ, that gives a simplified model for the vertical structure of the accretion disc. This work remained unnoticed for a long time.

In 1981, in a workshop on the cataclysmic variables, Jim Pringle discussed that the equilibrium solutions form an S-shaped curve on the $T_{\rm eff} - \Sigma$ plane (Fig. 2.1) and could explain the DN outbursts. $T_{\rm eff}$ at a given radius r is also a measure of the mass-flow rate, $\dot{M}$, at that radius. The upper and lower branches of the S-curve with positive slopes are stable, while the middle branch with a negative slope is unstable. At a given r, if the disc is at some point on the lower branch, $\Sigma(r)$ increases due to low temperature and thus low kinematic viscosity, ν. This branch is called the cold state. Eventually, Σ reaches the $\Sigma_{\rm max}$ (see Fig. 2.1), temperature and $\dot{M}$ suddenly increase to the point on the upper branch corresponding to $\Sigma_{\rm max}$. In the hot state (upper branch), Σ decreases due to high viscosities and $\dot{M}$. When Σ decreases to $\Sigma_{\rm min}$ at the lowest point of the upper branch, the matter at this r makes a transition back to the point on the lower branch corresponding to $\Sigma_{\rm min}$. How does this mechanism give rise to an X-ray outburst? When the disc at a radius r makes a transition to the hot state, a heating front propagates to both inner and outer radii. If a large fraction of the disc makes a transition to the hot branch with this propagation of the heating front, then the resultant increase in the mass-flow rate from the outer to the inner disc leads to an abrupt increase in $L_{\rm X}$, starting the

X-ray outburst.

Figure 2.1 Temperature - Surface density diagram (S-Curve)

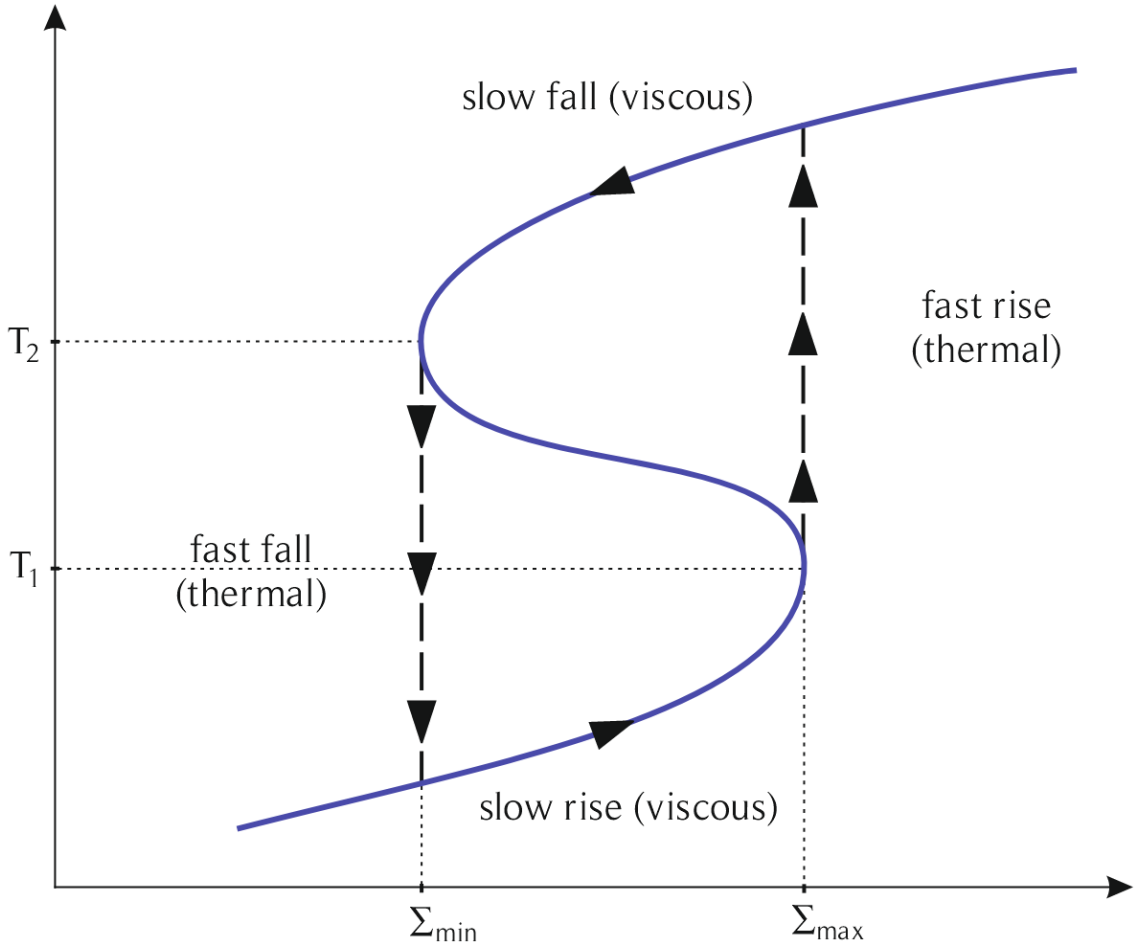

The disc instability model (DIM) can explain DN light curves with time-scales much shorter than those of NSXTs and BHXTs. Assuming that the disc is heated only by viscous dissipation, this model cannot explain the long outburst durations and recurrence times of NSXTs with the kinematic viscosity parameters similar to those used for DNs. Accretion discs of NSXTs, BHXTs and DNs are estimated to have similar chemical compositions. Therefore, a reasonable model should yield the outburst light curves of NSXTs and BHXTs with viscosity parameters comparable to those that can reproduce DN outburst light curves. It was proposed that the X-ray irradiation should be taken into account to explain the X-ray outburst characteristics of X-ray transients (van Paradijs, 1996). This idea was later supported by detailed analytical and numerical calculations (Dubus et al., 2001, 1999; Frank et al., 2002; King, 1998; King & Ritter, 1998). For a white dwarf with a radius 1000 times greater than a NS, the X-ray luminosity is too weak to heat the disc, while for NS or BH systems, it is the dominant heating mechanism for the outer disc.

3. APPLICATION TO AQL X-1

Sections 3.1, 3.2, and 3.4 in this chapter are included in our work that has been submitted to a scientific journal.

3.1 Introduction

Low-mass X-ray binaries (LMXBs) are systems containing either a neutron star (NS) or a black hole (BH) and a low-mass companion star with mass $M < 1M_{\odot}$. In LMXBs, mass is transferred from the companion to the compact object through Roche-lobe overflow. Due to its angular momentum, the matter cannot fall directly onto the star. Instead, the material forms a geometrically thin accretion disc around the NS (Frank et al., 2002). The matter in the disc moves in Keplerian orbits with speed $\upsilon_{\rm K} = (GM/r)^{1/2}$ where G is the gravitational constant, M is the mass of the NS, and r is the radial distance from the centre. Through viscous processes, angular momentum is carried outwards while the matter flows inwards toward the compact object.

A small fraction of these systems are persistent X-ray sources, while the remaining larger fraction consists of transient systems, with both neutron stars (NSXTs) and black holes (BHXTs) that show X-ray outbursts with large ranges of recurrence and duration time-scales (see e.g. Psaltis, 2006). The inner disc in NSXTs is cut at a radius, $r_{\rm in}$, depending on the mass inflow rate, $\dot{M}_{\rm in}$, of the disc and the dipole moment $\mu = BR_{*}^{3}$ of the NS, where B and R_{*} are the dipole field strength at the equator and the radius of the star respectively. At the co-rotation radius $r_{\rm co} = (GM/\Omega_{*}^{2})^{1/3}$, the angular speed of the NS, Ω_{*}, equals the Keplerian angular speed, $\Omega_{\rm K}$, of the disc matter. If $r_{\rm in} \leq r_{\rm co}$, the matter can flow from the inner disc along the closed field lines onto the NS. In the case that $r_{\rm in} > r_{\rm co}$, the matter is estimated to be thrown out from the inner disc (propeller effect; Illarionov & Sunyaev, 1975).

For a given μ, the critical $\dot{M}_{\rm in}$ level for the onset of the propeller mechanism is not well known. For spherical accretion onto a non-rotating magnetised star, magnetic pressure balances the ram pressure of the inflowing matter at Alfvén radius, $r_{\rm A} \simeq (GM)^{-1/7}\mu^{4/7}\dot{M}_{\rm in}^{-2/7}$ (Davidson & Ostriker, 1973; Lamb et al., 1973). In the case of disc accretion, $r_{\rm in}$ is conventionally estimated by equating the viscous and magnetic stresses and found to be $r_\xi = \xi r_{\rm A}$ with $\sim 0.5 < \xi < 1$ (Ghosh & Lamb, 1979; Kluźniak & Rappaport, 2007).

It was proposed that there is a minimum critical X-ray luminosity, $L_{\rm X}$, to become a persistent LMXB such that the entire disc is kept hot above the hydrogen ionisation temperature by the X-ray irradiation flux with an $L_{\rm X}$ above this critical level (van Paradijs, 1996). When $L_{\rm X}$ decreases below the critical rate, the outer cold regions of the disc enter a low viscosity state with an inefficient mass transfer from the outer to the inner disc with a rate lower than the mass-flow rate, $\dot{M}_{\rm c}$, from the companion to the outer disc. This leads to a gradual increase in the surface densities and temperatures of the outer disc. When the outer disc temperature exceeds the critical level at a radius, a heating front propagates to inner and outer radii, which could take most of the disc into the "hot state" with higher viscosities enhancing the mass transfer to the inner disc. The resultant abrupt increase in $\dot{M}_{\rm in}$ at the inner disc is observed as an X-ray outburst. In the outburst phase, efficient mass transfer from the outer radii decreases the surface densities and temperatures of the outer disc. Eventually, starting from the outer disc, propagation of a cooling front inward could take the entire disc into the "cold state" with much lower $\dot{M}_{\rm in}$ and $L_{\rm X}$ (quiescent state). To sum up, the outer disc behaves like a mass reservoir in the quiescent state, and this mass is released as a result of thermal-viscous disc instability producing an X-ray outburst (see e.g. Frank et al. 2002; Lasota 2001 for details).

The $L_{\rm X}$ peak in outbursts and the recurrence time-scale, $\tau_{\rm rec}$, depend on the size of the disc together with the mass transfer rate from the companion, as well as the X-ray irradiation strength during the outburst. The X-ray irradiation slows down the inward propagation of the cooling front during the outburst state. Therefore, the outer disc of a system with relatively high $L_{\rm X}$ is evacuated more efficiently during outbursts, which needs a longer $\tau_{\rm rec}$ to refill the disc. For instance, $\tau_{\rm rec} \sim$ weeks for dwarf novae (DNs), while for NSXTs and BHXTs $\tau_{\rm rec}$ varies from months to decades (Frank et al., 2002).

In the disc instability models (DIMs), the disc diffusion equation is usually solved using the α-prescription of the kinematic viscosity $\nu = \alpha c_{\rm s} h$ (Shakura & Sunyaev, 1973), where $c_{\rm s}$ is the sound speed, and h is the pressure scale-height of the disc.

The basic characteristics of DN light curves can be reproduced with $\alpha_{\rm h} \simeq 0.1$ and $\alpha_{\rm c} \simeq 0.01 - 0.05$ for the hot and cold viscosity states, respectively. DIMs can also account for the outburst light curves and recurrence times of transient LMXBs with $\alpha_{\rm h}$ and $\alpha_{\rm c}$ values similar to those used for DNs provided that the effect of X-ray irradiation on the disc dynamics during the outburst states is included in the models (Dubus et al., 2001, 1999; King, 1998; King & Ritter, 1998).

A characteristic "knee" followed by a steepening in the X-ray outburst light curves observed from a variety of magnetised stars in binaries including some NSXTs was proposed to be the signature of the onset of the propeller effect at a critical $L_{\rm X}$ corresponding to $r_\xi = \xi r_{\rm A} = r_{\rm co}$ with $\xi \simeq 0.5$ (Campana et al., 2018). Among these NSXTs, Aql X-1 is a prototypical source, accreting matter from a K-type companion. The spin period of the source $P = 1.8$ ms (Casella et al., 2008). In quiescence, $L_{\rm X} \simeq 5 \times 10^{33}$ erg s^{-1} for a distance $d = 4.5$ kpc (Campana et al., 2014; Galloway et al., 2008). In the outburst states, the $L_{\rm X}$ peak can exceed 10^{37} erg s^{-1} within a few days (Campana et al., 2013). After the peak of a typical outburst of Aql X-1, the X-ray light curve shows a smooth and slow exponential decay lasting a few weeks followed by a sharp turn downward, forming a knee-like morphology, and subsequently, $L_{\rm X}$ decreases more steeply down to the quiescent level within several days. The outbursts are repeated with a recurrence time $\tau_{\rm rec} \sim 1$ yr.

A steepening of the X-ray light curve during the decay phase is a behaviour estimated in the DIM resulting from the inward propagation of the cooling front (see e.g. King & Ritter 1998). Recently, Lipunova et al. (2022) showed through detailed numerical analysis that the knee in the decay curve of Aql X-1 could be produced as a result of the shrinking size of the hot inner disc during the decay phase of the outburst. Initially, the X-ray light curve is similar to that of a purely viscous relaxation (without disc instability). The presence of a cold-hot border is communicated to the innermost disc after a viscous time across the hot inner disc. While $r_{\rm h}$ is decreasing, the viscous time-scale of the hot disc also decreases. Below a critical level, this leads to a steeper $\dot{M}_{\rm in}$ and $L_{\rm X}$ decay compared to those in purely viscous decay. This sequence of events governed by the dynamics and viscous time-scale of the inner hot disc cause a transition from a slower to a faster decay in $L_{\rm X}$, producing a knee-like morphology in the X-ray outburst light curve. In their model, to account for the sharp decay, Lipunova et al. (2022) included a partial accretion regime when $r_{\rm in} > r_{\rm co}$ with a varying accretion fraction depending on the fastness parameter, $(r_{\rm in}/r_{\rm co})^{3/2}$, adopting $r_{\rm in} = r_\xi$ (see the discussion in Sec. 3.2).

In this work, we also investigate the X-ray outburst light curves of Aql X-1 together with its recurrence characteristics in the frame of DIMs. In our model, the physical

reason for the formation of the knee is similar to that found by Lipunova et al. (2022), while the functional form of the sharp decay after the knee is produced in a way rather different from the mechanism adopted in Lipunova et al. (2022). Without including partial accretion or a strong propeller in the model, we have shown that the sharp $L_{\rm X}$ decay can be accounted for by taking the weak $\dot{M}_{\rm in}$ dependence of the disc aspect ratio, h/r, into account in the X-ray irradiation flux calculations. In the model, repeating outbursts with similar X-ray outburst light curves and with a recurrence time in agreement with the observations can also be reproduced. We briefly describe our model in Section 3.2. After a parameter study in Section 3.3, we discuss the results of the model calculations in Section 3.4.

3.2 Model

We use the numerical code employed earlier by Ertan & Alpar (2002) to simulate the fast-rise-exponential-decay (FRED) type outburst light curves of BHXTs. Here, we briefly describe the model calculations.

We represent the mass distribution of the disc before the X-ray outburst with a Gaussian surface density distribution $\Sigma(r,t=0)=\Sigma_0\exp\Big[-\Big\{(r-r_{\rm circ}/\Delta r\Big\}^2\Big]$ centred at the circularisation radius, $r_{\rm circ}$. Through numerical calculations, we solve the diffusion equation

$$\frac{\partial\Sigma}{\partial t}=\frac{3}{r}\frac{\partial}{\partial r}\left[r^{1/2}\frac{\partial}{\partial r}(\nu\Sigma r^{1/2})\right] \tag{3.1}$$

(Frank et al., 2002) to calculate $\Sigma(r,t)$ together with corresponding $\dot{M}_{\rm in}$ evolution. We use the α prescription of the kinematic viscosity, $\nu=\alpha c_{\rm s}h$ (Shakura & Sunyaev, 1973) where $h=c_{\rm s}\Omega_{\rm K}$ is the pressure scale height of the disc, $c_{\rm s}=\sqrt{k_{\rm B}T_{\rm c}/\mu m_{\rm p}}$ is the sound speed, $m_{\rm p}$ is the proton mass, μ is the mean molecular weight in units of $m_{\rm p}$, and $T_{\rm c}$ is the mid-plane temperature of the disc. For a better resolution of the inner disc, we solve the diffusion equation substituting $x=2r^{1/2}$ and $S=x\Sigma$ (Frank et al., 2002). We divide the disc into 800 radial grids equally spaced in x-space.

The viscous dissipation rate per unit disc area (from the mid-plane to the surface of the disc) can be written as

$$D(r)=\frac{9}{8}\nu\Sigma\frac{GM}{r^3}=\frac{4\sigma}{3\tau}T_{\rm c}^4 \tag{3.2}$$

where σ Stephan-Boltzmann constant, and $\tau = \kappa\Sigma$ is the vertically integrated optical depth of the disc. For an optically thick, geometrically thin disc, $\tau \gg 1$, and the dissipated energy is emitted locally in the form of blackbody radiation. We use the Rosseland mean opacities from the opacity tables for population I stars (Alexander & Ferguson 1994, for $\log T \leq 3.7$ and Iglesias & Rogers 1996, for $\log T > 3.7$).

In addition to viscous dissipation, the disc is also heated by the X-rays produced by the accretion onto the NS. The X-ray irradiation flux for a point source is given by

$$F_{\rm irr} = \sigma T_{\rm irr}^4 = \frac{\eta \dot{M}_* c^2 (1-\epsilon)}{4\pi r^2} \frac{h}{r} \left(\frac{{\rm d}\ln h}{{\rm d}\ln r} - 1 \right) = C \frac{\dot{M}_* c^2}{4\pi r^2} \tag{3.3}$$

(Dubus et al., 1999; Shakura & Sunyaev, 1973) where η is the efficiency of the conversion of rest mass energy into radiation and ϵ is the X-ray albedo (fraction of matter scattered from disc surface without absorption) of the disc surface, and

$$C \equiv \eta(1-\epsilon) \frac{h}{r} \left(\frac{{\rm d}\ln h}{{\rm d}\ln r} - 1 \right) \tag{3.4}$$

is the irradiation parameter which is estimated to be in the range of $10^{-4} - 10^{-3}$ from the model fits to the optical and X-ray spectra of LMXBs (De Jong et al., 1996; Dubus et al., 1999; Ertan & Alpar, 2002). Note that if $F_{\rm irr}$ is defined in terms of $L_{\rm X} = \eta \dot{M}_* c^2$, then the irradiation parameter becomes greater than C given by Eqn. (3.4) by a factor of $1/\eta$.

The effective temperature of the disc $T_{\rm eff} \simeq [(D + F_{\rm irr})/\sigma]^{1/4}$. At the inner disc regions, D dominates $F_{\rm irr}$, while outside a radius ($\sim 10^9$ cm) the X-ray irradiation is the dominant heating mechanism. Since the h/r ratio in the Eqn. (3.4) is not very sensitive to $\dot{M}_{\rm in}$ and $r\left(h/r \propto \dot{M}_{\rm in}^{3/20} r^{1/8}\right)$, it seems reasonable to take C constant in the calculations (Frank et al., 2002). Nevertheless, in our simulations, we noticed that the variation of h/r with $\dot{M}_{\rm in}$ and the resultant change in $F_{\rm irr}$ significantly modify the slope of the X-ray light curve in the sharp decay phase after the knee. Including the weak $\dot{M}_{\rm in}$ and r dependence of h/r, equation (3.4) can be written as

$$C = C_0 \, \dot{M}_{*,17}^{3/20} \, r_{10}^{1/8} \tag{3.5}$$

where $\dot{M}_{*,17} = (\dot{M}_*/10^{17}$ g s$^{-1})$, $r_{10} = (r/10^{10}$ cm), and C_0 will be a free parameter of our model.

Following the conventional approach, we calculate the kinematic viscosity with two different α parameters, $\alpha_{\rm h}$ and $\alpha_{\rm c}$, for the hot and cold viscosity states, respectively. For a given r in the cold (hot) state, there is a maximum (minimum) critical surface

density $\Sigma_{\rm max}$ ($\Sigma_{\rm min}$) for the transition to the hot (cold) state. We adopt $\Sigma_{\rm max}$ and $\Sigma_{\rm min}$ equations obtained by Dubus et al. (2001) through detailed vertical disc analyses. Interpolating the critical Σ values found for different radii of the disc, Dubus et al. (2001) obtained

$$\Sigma_{\rm max} = (10.8 - 10.3\,\xi)\,\alpha_{\rm c}^{-0.84}\ M_1^{-0.37+0.1\xi}\ r_{10}^{1.11-0.27\xi}\ {\rm g\,cm^{-2}}, \tag{3.6}$$

$$\Sigma_{\rm min} = (8.3 - 7.1\,\xi)\,\alpha_{\rm h}^{-0.77} M_1^{-0.37}\ r_{10}^{1.12-0.23\xi}\ {\rm g\,cm^{-2}} \tag{3.7}$$

where $\xi = (T_{\rm irr}/10^4\ {\rm K})^2$, and M_1 is the mass of the NS in solar masses. For our initial mass distribution, $L_{\rm X} \simeq 0$ until the surface densities increase at the inner disc, which is not realistic since $L_{\rm X}$ does not decrease below the quiescence level. Considering these situations, in addition to the critical surface densities, we also impose the $\alpha = \alpha_{\rm h}$ condition for radii at which $T_{\rm eff} > 6000$ K, independent of $T_{\rm irr}$.

The X-ray luminosity produced by accretion onto the star is related to the total disc luminosity through

$$L_{\rm acc} \simeq \frac{GM\dot{M}_*}{R_*} \simeq \frac{2r_{\rm in}}{R_*}\ L_{\rm disc} \tag{3.8}$$

when $r_{\rm in}$ is not close to R_*. A large fraction of the disc luminosity is emitted from the innermost disc regions. In our numerical calculations, we take $r_{\rm in} = r_{\rm co}$, and $\dot{M}_* = \dot{M}_{\rm in}$ throughout the outburst state. The exact position of $r_{\rm in}$ does not significantly affect the $\dot{M}_{\rm in}$ evolution.

The maximum inner disc radius at which a steady propeller mechanism can be established could be written as

$$R_{\rm in,max}^{25/8} \left|1 - R_{\rm in,max}^{-3/2}\right| \ \simeq\ 1.26\ \alpha_{-1}^{2/5}\ M_{1.4}^{-7/6}\ \dot{M}_{\rm in,16}^{-7/20}\ \mu_{30}\ P^{-13/12} \tag{3.9}$$

(Ertan, 2017,1), where $R_{\rm in,max} = r_{\rm in,max}/r_{\rm co}$, $M_{1.4} = (M/1.4M_\odot)$, $\dot{M}_{\rm in,16} = (\dot{M}_{\rm in}/10^{16}\ {\rm g\ s^{-1}})$, $\mu_{30} = (\mu/10^{30}\ {\rm G\ cm^3})$, $\alpha_{-1} = (\alpha/0.1)$, and P is the spin period of the NS. Ertan (2017) derived this formula through analytical calculations adopting the basic results of the disc-magnetosphere interaction model proposed by Lovelace et al. (1995), which was developed later to simulate the propeller phase as well (Lovelace, Romanova & Bisnovatyi-Kogan, 1999; Ustyugova et al., 2006). In this model, the inner disc settles down at a radius where the field lines can force the innermost disc matter into co-rotation. The inner disc-field interaction takes place in a narrow boundary with radial width $\Delta r < r$. The field lines interacting with matter inflate and open up within an interaction time-scale $\tau_{\rm int} = |\Omega_{\rm K} - \Omega_*|^{-1}$. In

the propeller phase, the matter can be thrown out along the open field lines. Subsequently, the lines reconnect on a time-scale similar to $\tau_{\rm int}$. The field lines outside the boundary are open and decoupled from the disc. With these conditions, Ertan (2017) found that the inflowing disc matter can be stopped at $r_{\rm A}$ but cannot be thrown out from the system efficiently. The resultant pile-up pushes the inner disc inwards to the radius at which the field is strong enough to expel all the inflowing mass from the inner disc, continuously evacuating the inner boundary. Equation (3.9) gives the maximum radius at which this strong propeller condition is satisfied. In the propeller phase, $r_{\rm in} = r_\eta$ does not scale with and in some cases significantly smaller than $r_{\rm A}$ (see Ertan 2017,1,2 for details).

The actual inner disc radius is estimated to be close to $r_{\rm in,max}$, and can be written as $r_\eta = \eta r_{\rm in,max}$ where η is a parameter close to unity. The $L_{\rm X}$ level corresponding to strong propeller/accretion transition can be estimated from Eqn. (3.9). The predictions of this model for the critical $L_{\rm X}$ and the torque variations are in agreement with the properties of transitional millisecond pulsars (tMSPs; see Papitto & Martino 2022 for a recent review) during their transitions between the LMXB and the radio millisecond pulsar (RMSP) states (Ertan, 2017,1). The model was recently developed to include all the rotational phases of the NSs in LMXBs (Ertan, 2021) and applied to the torque-reversal properties of LMXBs as well (Gencali et al., 2022). In this work, we use Eqn. (3.9) to estimate the dipole field strength of Aql X-1 that is consistent with the results of our X-ray light curve analysis.

We also perform simulations to analyse and compare the repeating outburst light curves produced in the model with the observed recurrent outbursts of Aql X-1. To represent the mass flow from the companion, we add mass into the radial grid at $r_{\rm circ}$ at each time step. For Aql X-1, $r_{\rm co} \simeq 2.5 \times 10^6$ cm, $r_{\rm circ} = 5.0 \times 10^{10}$ cm, and we take $r_{\rm out} = 1.8 \times 10^{11}$ cm in our calculations. We have repeated the numerical calculations with different mass-flow rates, $\dot{M}_{\rm c}$, from the companion until we obtain typical outburst morphology and recurrence time of Aql X-1. In Sec. (3.4), we discuss the results of the model calculations summarised above.

3.3 Parameter Study

In this section, we will examine how the disc parameters $\alpha_{\rm c}$, $\alpha_{\rm h}$, C, and the initial disc mass $M_{\rm disc}$ affect the X-ray outburst light curve morphology. We will also test

how the details of initial mass distribution for a given $M_{\rm disc}$ change the outburst light curve characteristics. We represent the mass accumulated along the quiescent state (before the disc instability is triggered) by a Gaussian distribution as described in Sec. 3.2.

For all the illustrative numerical calculations here, we take $r_{\rm in} = 2.5 \times 10^6$ cm, $r_{\rm circ} = 5 \times 10^{10}$ cm, $r_{\rm out} = 1.8 \times 10^{11}$ cm, and the mass and radius of the NS $M = 1.4 M_\odot$ and $R = 10^6$ cm, respectively.

Simulation 1: For comparison with subsequent simulations, we perform the first simulation with an illustrative set of parameters: $M_{\rm disc} = 2 \times 10^{24}$ g, $\Delta r = 10^9$ cm, $\alpha_{\rm h} = 0.1$, $\alpha_{\rm c} = 0.01$, and $C = 2 \times 10^{-4}$. We use the critical conditions described in Sec. (3.2) for the transitions between the cold and hot viscosity states. The model curve obtained with these parameters is seen in Fig. (3.1).

Figure 3.1 The X-ray outburst light curve produced by simulation 1 (top panel). The bottom panel shows the variation of $r_{\rm h}$ during the outburst. The model parameters are: $\alpha_{\rm h} = 0.1$, $\alpha_{\rm c} = 0.01$, $C = 2 \times 10^{-4}$ and $M_{\rm disc} = 2 \times 10^{24}$ g.

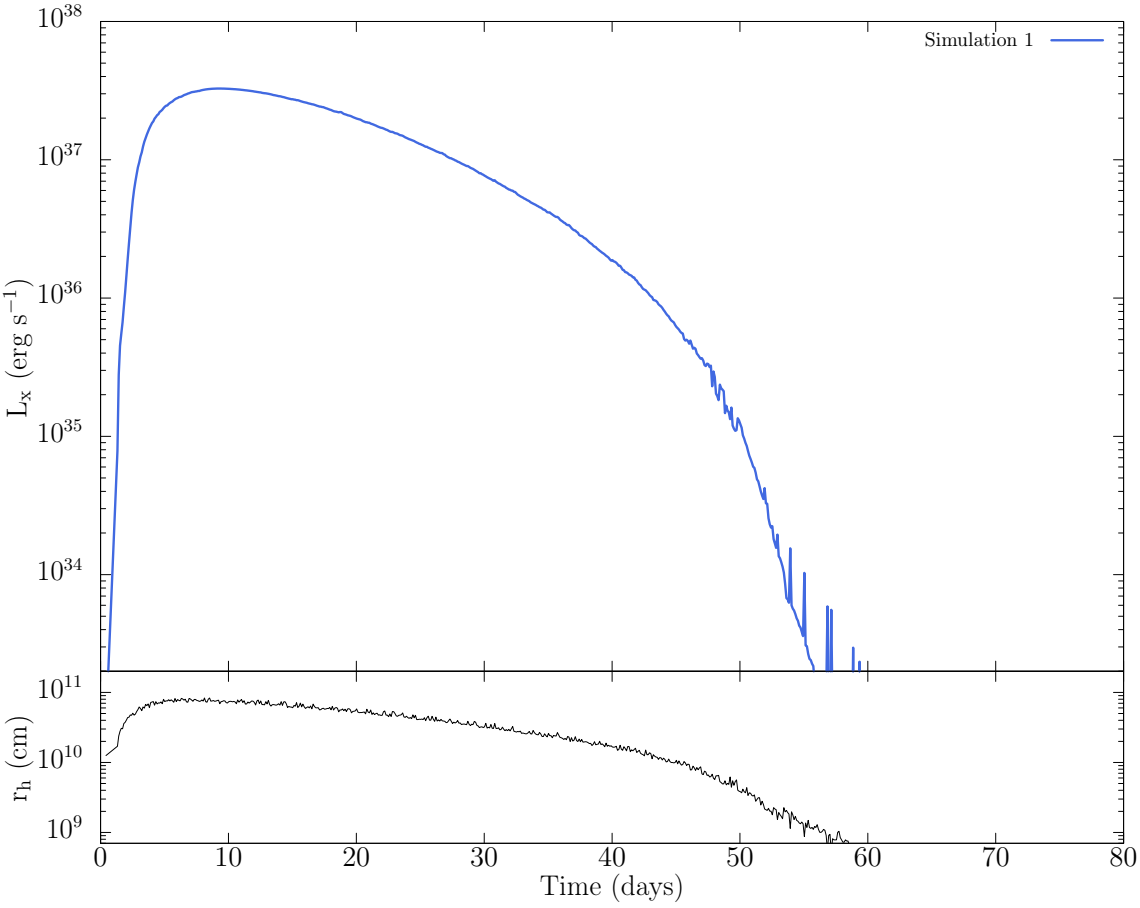

As shown in Fig. (3.1), $L_{\rm X}$ reaches its peak with an abrupt increase within a few days. After the peak, the initial exponential decay time-scale is a few weeks. The

outer radius of the hot disc, $r_{\rm h}$, decreases with decreasing $L_{\rm X}$. The mass inflow rate at the cold regions that remains outside $r_{\rm h}$ decreases. This effect starts to modify the $L_{\rm X}$ curve after $r_{\rm h}$ decreases below $\sim 10^{10}$ cm (at t $\sim$ 40 days in Fig. 3.1) leading to a sharper decay starting from $L_{\rm X} \sim 10^{36}$ erg s^{-1} to the quiescent level within a few days.

Simulation 2: Different initial mass distributions with the same $\mathbf{M_{disc}}$. In this simulation, we try different $\Delta r - \Sigma_0$ pairs for the same $M_{\rm disc}$ to see how the details of the initial mass distribution affect the model light curve. The other model parameters are the same as those used in the first simulation.

Figure 3.2 Model curves for different initial mass distributions. Δr and Σ_0 values are given in the figure. The initial disc mass $M_{\rm disc} = 2 \times 10^{24}$ g is the same for the three illustrative models. The dotted line is the model curve obtained in simulation 1 Fig. (3.1).

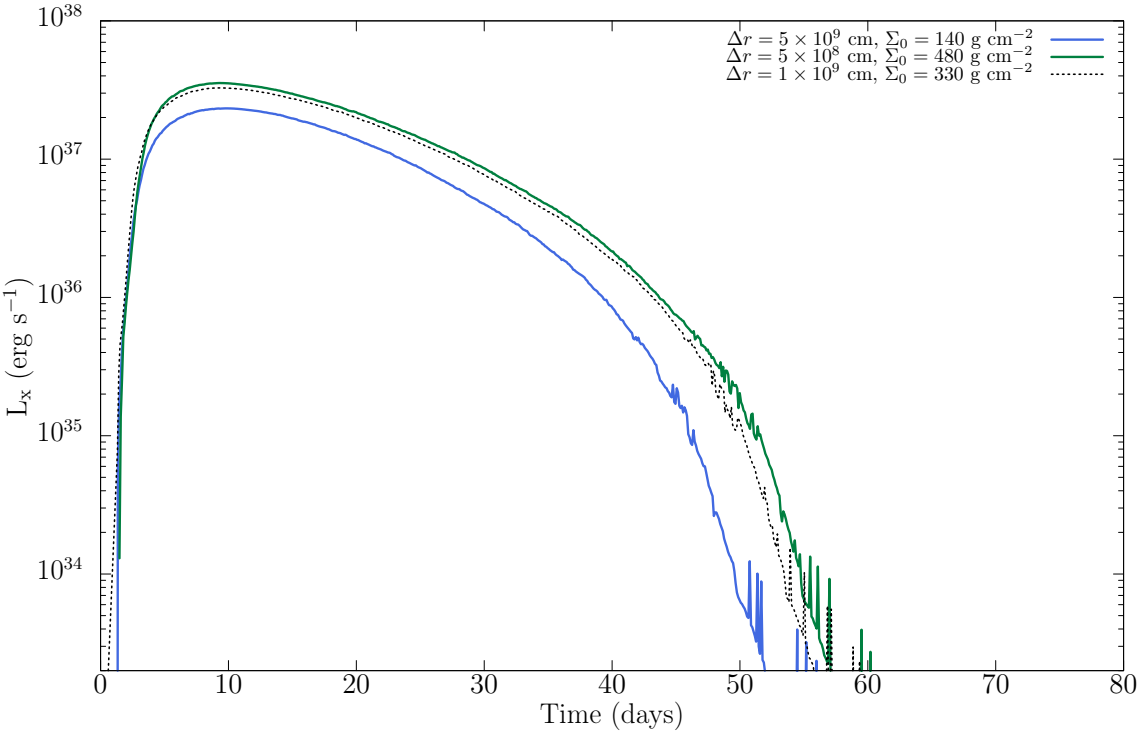

The initial mass distribution with higher Δr is more extended along the disc. During the outburst, the distribution with a relatively narrow Δr spreads to smaller and larger radii more rapidly due to its higher Σ gradients producing a higher $L_{\rm X}$ peak, heating the disc to a larger radius. Therefore, the initial Σ distribution with narrower Δr yields an outburst with a greater fluence. Nevertheless, it is seen in Fig. (3.2) that outburst light curves produced by these rather different initial Σ_0 do not show any significant differences in their light curve morphology (rise time, exponential decay, steepness of the decay).

Simulation 3: Different initial disc masses. The model curves seen in Fig. (3.3) are obtained with three different Σ_0 values (given in the figure), while all the other parameters are the same as in simulation 1. The outburst with a greater $M_{\rm disc}$ has a higher $L_{\rm X}$ peak since there is more material to accrete onto the compact star along the outburst phase. For the most massive disc, the entire disc up to $r_{\rm out}$ is taken into the hot state due to a stronger $F_{\rm irr}$, unlike the case for the simulations with smaller $M_{\rm disc}$. In the case of greater $M_{\rm disc}$, higher viscosities results in a sharper and higher peak in the X-ray outburst light curve. Due to efficient X-ray irradiation, the initial exponential decay phase also lasts longer.

For the smallest $M_{\rm disc}$, the $L_{\rm X}$ curve also increases rapidly in the first few days. However, this curve never enters the initial exponential decay phase due to a low $L_{\rm X}$ peak with an $F_{\rm irr}$ that is insufficient to heat the disc to radii greater than $\sim 10^{10}$ cm. Remarkably, the three curves decay with the same slope below $L_{\rm X} \sim 10^{35}$ erg s^{-1}.

Figure 3.3 Illustrative model curves for different disc masses. The blue and green solid lines are obtained with $M_{\rm disc} = 6 \times 10^{24}$ g and $M_{\rm disc} = 6.7 \times 10^{23}$ g, respectively. The dotted line is the model curve obtained in the first simulation.

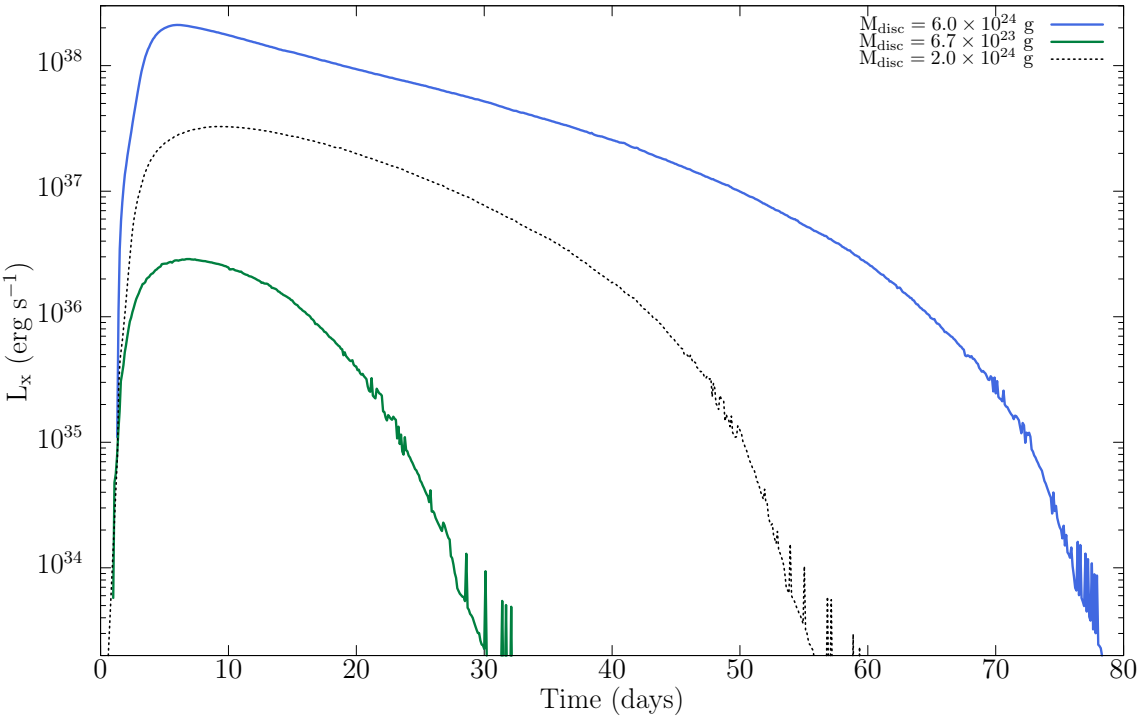

Simulation 4: Kinematic viscosity parameter, $\alpha_{\rm h}$. In this simulation, we try different kinematic viscosity parameter values, $\alpha_{\rm h}$, to see their effects on the light curves. The illustrative model curves seen in Fig. 3.4 are obtained with $\alpha_{\rm h} = 0.15$ (solid blue line) and $\alpha_{\rm h} = 0.08$ (solid green line).

The effect of changing $\alpha_{\rm h}$ is rather straightforward. The disc with higher $\alpha_{\rm h}$ has a

higher ν and a shorter viscous time-scale; therefore, more matter accretes onto the star in a shorter time interval, yielding an outburst with a higher $L_{\rm X}$ peak. With a lower $\alpha_{\rm h}$, the viscous time-scale is longer. In the outburst state, the mass-flow rate along the hot disc is low, which prolongs the duration of the outburst state.

Figure 3.4 Model curves for different $\alpha_{\rm h}$ parameters. The blue and green solid lines represent the results with $\alpha_{\rm h} = 0.15$ and $\alpha_{\rm h} = 0.08$, respectively. The dotted line shows the model curve obtained in Fig. (3.1).

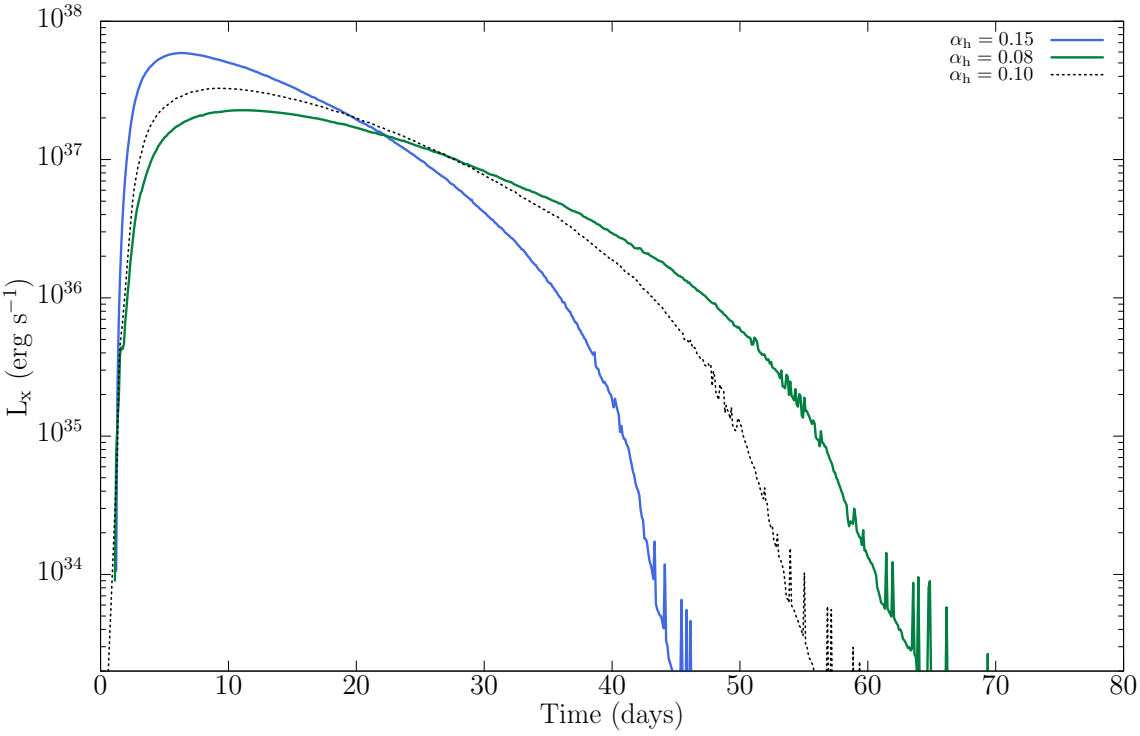

Simulation 5: Kinematic viscosity parameter, $\alpha_{\rm c}$. In this simulation, we compare the model curves obtained with different $\alpha_{\rm c}$ values (given in Fig. 3.5). For a smaller $\alpha_{\rm c}$, the critical $\Sigma_{\rm max}$ values are higher, requiring a longer time interval to trigger disc instability and produce an outburst. The model X-ray outburst curves obtained with different $\alpha_{\rm c}$ values do not show significant differences because it is mainly the hot state viscosities and $F_{\rm irr}$, rather than $\alpha_{\rm c}$, that govern the $L_{\rm X}$ evolution during an X-ray outburst. The similarity between the outburst light curve morphologies obtained with different $\alpha_{\rm c}$ values is seen in Fig. (3.5).

Figure 3.5 Model curves for different α_c parameters. The solid blue line is produced with $\alpha_c = 5 \times 10^{-3}$. The dotted line shows the model curve obtained in simulation 1 with $\alpha_c = 1 \times 10^{-2}$ (Fig. 3.1).

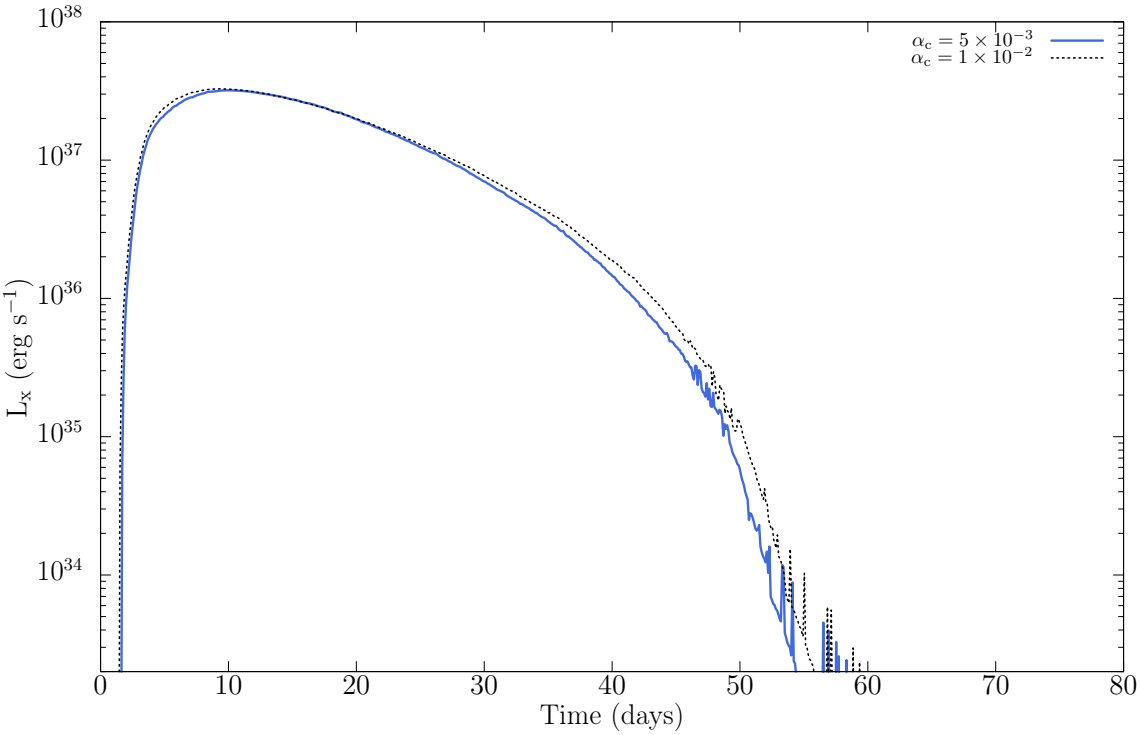

Simulation 6: The irradiation strength. In this simulation, we test the effect of the X-ray irradiation strength on the outburst light curve. The blue model curve in Fig. (3.6) is obtained by a C parameter two times greater than that producing the dotted model curve (simulation 1). The other parameters are the same for the two models. The solid blue line reaches a higher L_X peak, and its initial exponential decay lasts longer than the decay of the dotted curve. For a source with stronger F_{irr}, the cooling front is initially pushed back to a larger r, and its inward propagation takes a longer time. In this case, more matter flows onto the star for a longer period creating a brighter and longer outburst.

Figure 3.6 Model curves for different irradiation strengths. We obtain the solid and dotted lines with $C = 4 \times 10^{-4}$ and $C = 2 \times 10^{-4}$, respectively. The dotted line shows the model curve obtained in reference simulation 1 (Fig. 3.1).

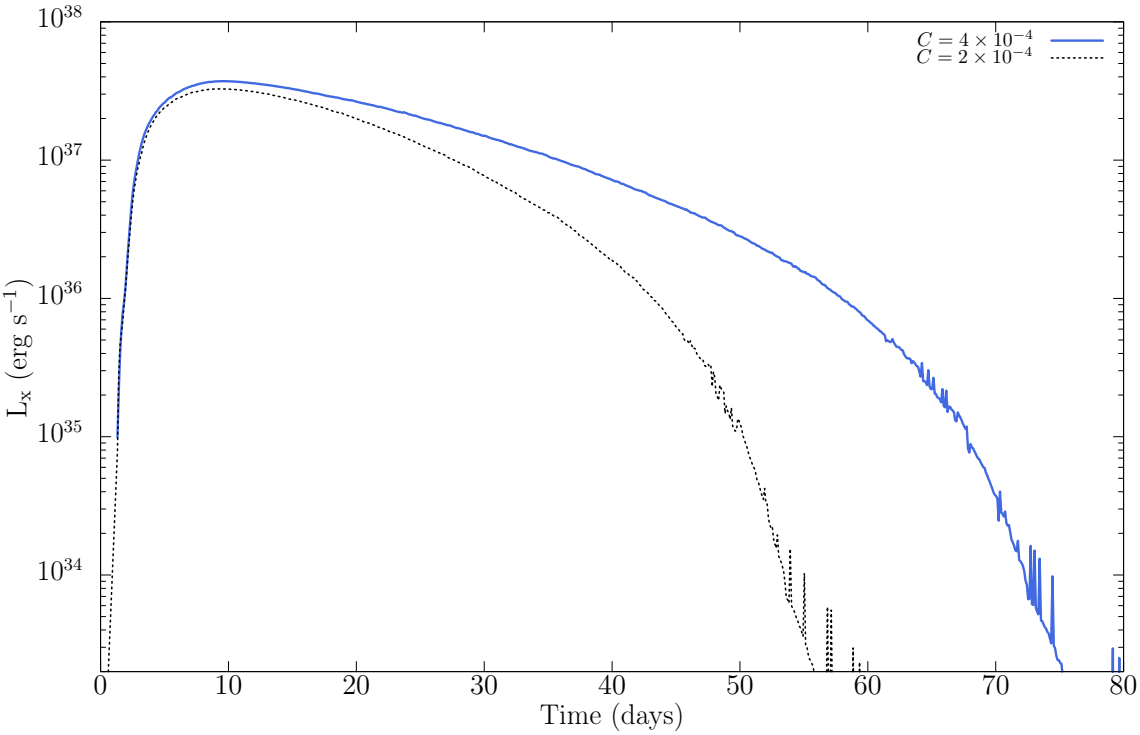

Simulation 7: Effect of $F_{\rm irr}$ with varying h/r ratio on the X-ray outburst light curve. In this simulation, we include the weak $\dot{M}$ and r dependences of the h/r ratio in the calculation of the irradiation parameter C as described in Eqn. (3.5). The remaining parameters are the same as in the first simulation. This significantly changes the outburst light curve morphology compared with the model curves produced with constant h/r. The solid blue curve in Fig. (3.7) shows the model light curve governed by $F_{\rm irr}$ with varying disc aspect ratio, while the dotted curve is the model light curve produced with constant C. For both models, $L_{\rm X}$ curves show similar rise phases with time-scales of a few days. The differences between the decay curves of the two models could be interpreted as follows: $F_{\rm irr}$ is initially similar for both models taking a similar fraction of the disc into the hot state, which produces similar $L_{\rm X}$ peaks. Below $L_{\rm X} \sim$ a few 10^{36} erg s^{-1}, the X-ray light curve for *model a* (blue curve) shows a more rapid decline due to decreasing C with decreasing $\dot{M}$, unlike in *model b* (dotted curve). In this sharp decay phase, the middle disc regions cannot be evacuated efficiently because of the rapidly decreasing $r_{\rm h}$. In *model a*, the mass-flow rate from the cold disc region to the hot region becomes comparable to the mass accretion rate onto the star when $r_{\rm h}$ decreases to about a few 10^9 cm. The sharp decrease in $L_{\rm X}$ stops at the level corresponding to this mass accretion rate which depends mainly on the $\alpha_{\rm c}$ and the mass transfer rate $\dot{M}_{\rm c}$ from the companion.

The fluctuations around this level are due to disc instabilities around $r_{\rm h}$. The solid light curve is similar to the outburst light curve morphology of the Aql X-1 (see. Sec. 3.4).

The situation is somewhat different for *model b* with $F_{\rm irr}$ that remains relatively strong in the late decay phase of the outburst. This prolongs the duration of the outburst state. In this case, $L_{\rm X}$ could decrease to much lower rates at the end of the decay phase. Because the innermost part of the cold disc has been evacuated efficiently, providing a lower mass-flow rate into the inner hot disc.

Figure 3.7 X-ray irradiation with variable and constant h/r. In the top panel, solid and dotted lines show the model light curves produced by $\dot{M}$ dependent and constant irradiation parameters (see Sec. 3.2). The curves in the bottom panel show the $r_{\rm h}$ evolution during the outburst.

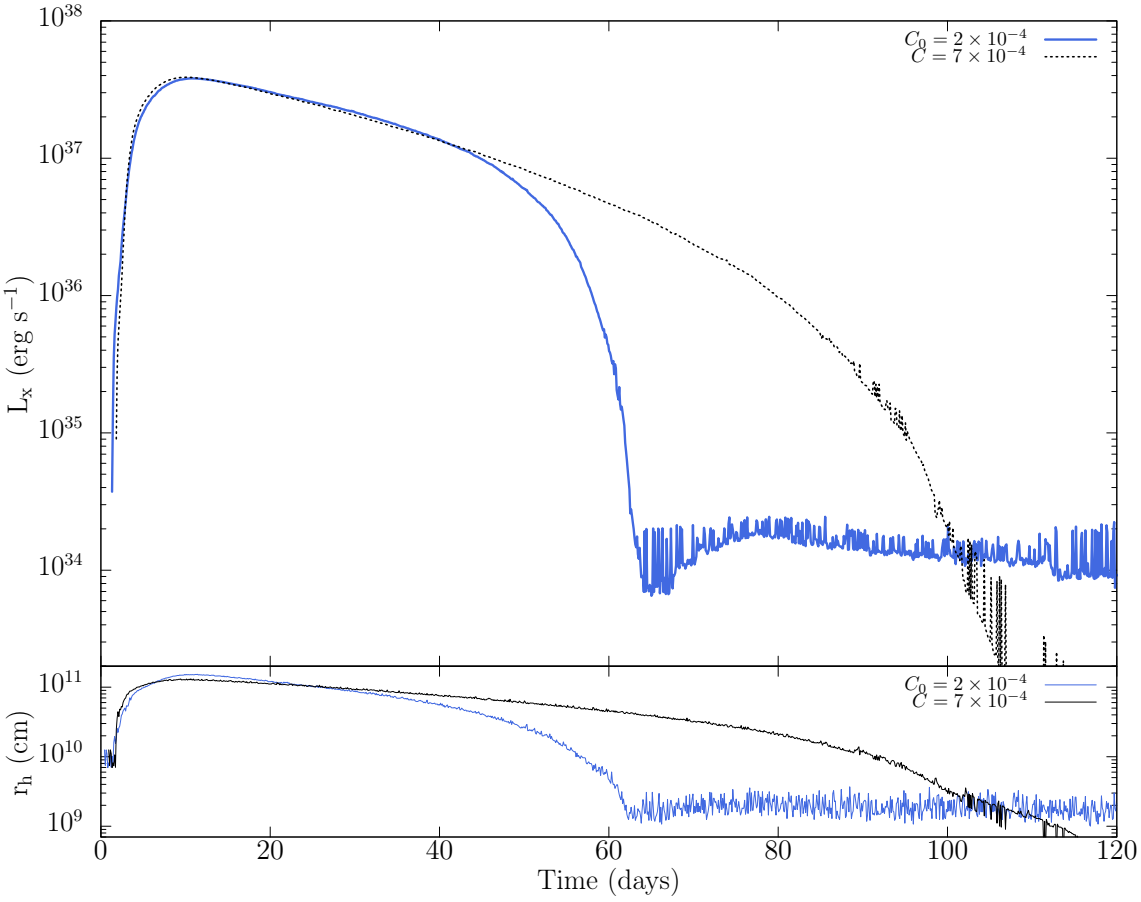

3.4 Results and Discussion

3.4.1 The 2010 Outburst of Aql X-1

The model curve in Fig. (3.8) is obtained with $\alpha_{\rm h} = 0.1$, $\mu = 0.6$ in the hot state, and $\alpha_{\rm c} = 5 \times 10^{-3}$, $\mu = 0.9$ in the cold state. The model can reproduce the basic features of the observed X-ray light curve with $C_0 \simeq 1.3 \times 10^{-4}$. The fluctuations seen in the decay phase are not addressed in our model. Therefore, a seemingly good fit to data is sufficient for our purpose in this work.

The sharp decay in $L_{\rm X}$ starts when $r_{\rm h}$ decreases to about 10^{10} cm. After the knee, the model cannot account for the functional form of the sharp decay curve without including the local $\dot{M}$ dependence of the h/r ratio, and its effect on $F_{\rm irr}$. We smooth out the realistic opacities to prevent numerical fluctuations. The $L_{\rm X}$ fluctuations during the quiescent state are due to continuous mass flow toward the inner region of the cold outer disc and the resultant local instabilities continually taking part of this region into the hot state. We calculate the entire $L_{\rm X}$ curve with $\dot{M}_* = \dot{M}_{\rm in}$. That is, $L_{\rm X}$ is produced by accretion onto the star without invoking any partial accretion or strong propeller. In this case, we can estimate an upper limit for the dipole field strength B on the surface of the star. Using Eqn. (3.9) and the strong propeller condition $r_\eta > 1.26 r_{\rm co}$ (see Ertan 2021 for details), the minimum $\dot{M}_{\rm in}$ level of the source ($\sim 3 \times 10^{13}$ g s^{-1}) gives $B < 2.3 \times 10^8$ G.

The model agrees with the observed $L_{\rm X}$ level in quiescence as well. The observed $L_{\rm X}$ is not smooth in quiescence. There are flares with ten-fold variations (Bernardini et al., 2013; Coti Zelati et al., 2014). These $L_{\rm X}$ fluctuations are also seen in our model curve. Nevertheless, accurate modelling of this behaviour is not easy due to the resolution problem for the innermost disc for a disc size greater than 10^{11} cm, which is beyond the scope of this work. We should also note that there are differences in the observed $L_{\rm X}$ levels after different outbursts (Campana et al., 2014).

Figure 3.8 X-ray outburst light curve of Aql X-1 (taken from Campana et al. (2014)). The solid model curve is obtained with $\alpha_{\rm c} = 5 \times 10^{-3}, \alpha_{\rm h} = 0.1, \mu_{\rm c} = 0.9, \mu_{\rm h} = 0.6$, and $C_0 = 1.3 \times 10^{-4}$. For the $L_{\rm X}$ calculation, we take $\dot{M}_* = \dot{M}_{\rm in}$ for the entire model curve.

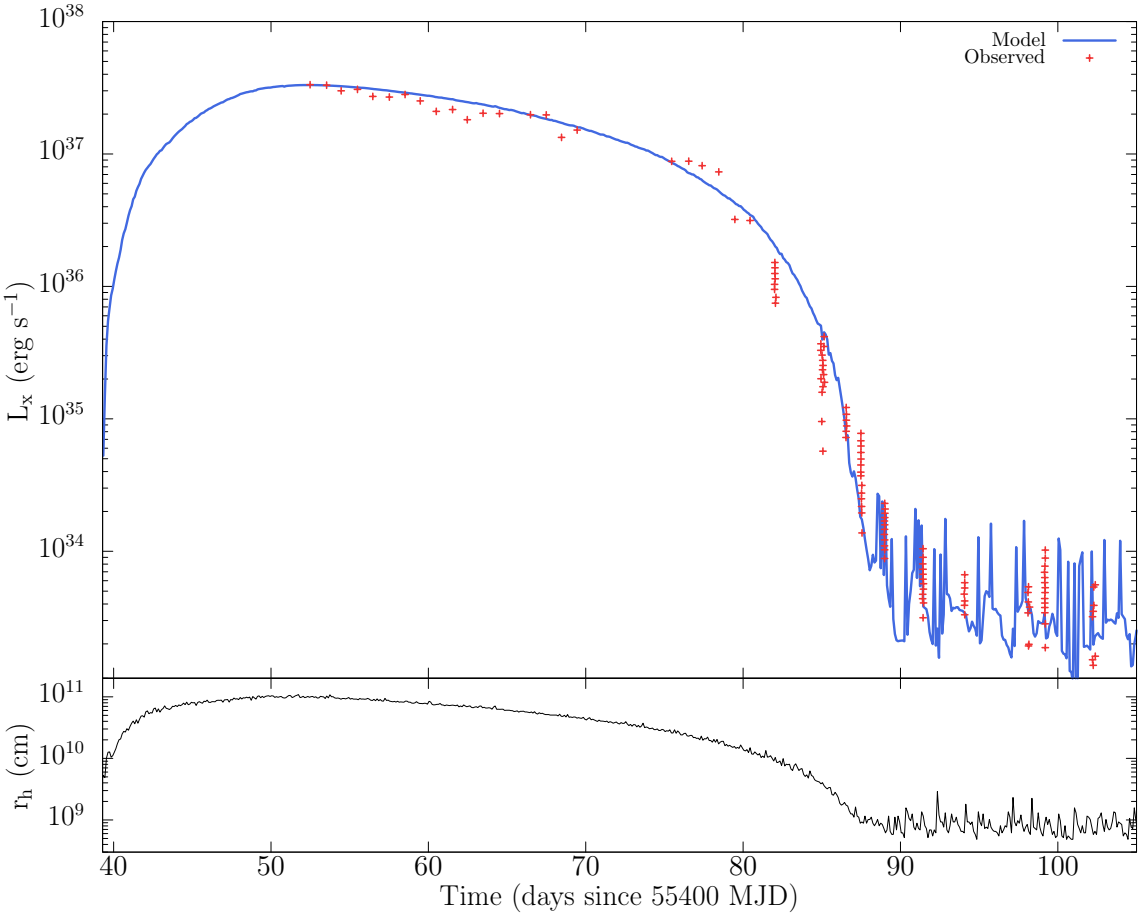

3.4.2 The Quiescent State and Recurrent Outbursts

Using the same model parameters producing the model curve in Fig. (3.8), we have continuously added mass into the radial grid at $r_{\rm circ} = 5 \times 10^{10}$ cm to represent the mass flow into the outer disc from the companion. The outburst light curves seen in Fig. (3.9) are obtained with $\dot{M}_{\rm c} = 4 \times 10^{16}$ g s^{-1} which produces outbursts with $\tau_{\rm rec} \sim 1$ year. It is interesting that the model light curves of the second and fourth outbursts also seemingly fit well to the X-ray outburst data of Aql X-1. For instance, Fig. (3.10) zooms in on the second outburst seen in Fig. (3.9). Simulations with higher values of $\alpha_{\rm c}$ produce outburst light curves with different morphologies, including those similar to the light curve seen in Fig. (3.8).

In the quiescent state of Aql X-1, $L_{\rm X} \simeq 5 \times 10^{33}$ erg s^{-1}. For comparison,

tMSPs are estimated to accrete matter from the disc down to $L_{\rm X}$ levels of $\sim 10^{33}$ erg s^{-1} (Archibald et al., 2009; Bassa et al., 2014; Papitto & Martino, 2022). Below this level, X-ray pulses are switched off, and they show RMSP behaviour. Dipole field strengths of tMSPs seem to be similar to that indicated by the upper limit $B < 2.3 \times 10^8$ G estimated for Aql X-1 in this work. Considering also the similarities in the rotational properties, Aql X-1 could have a critical $\dot{M}_{\rm in}$ rate for termination of accretion and transition to the propeller phase that is similar to that of tMSPs. This might be the reason for the lack of radio pulsations from Aql X-1 during its quiescent state. It is important to note here that the minimum pulsed $L_{\rm X}$ level of tMSPs is about two orders of magnitude smaller than the rate corresponding to $r_\xi = r_{\rm co}$.

Figure 3.9 The same model parameters are used for the solid curve in Fig. (3.8). This model curve is obtained by injecting mass into the radial grid at $r = r_{\rm circ}$ with a rate of 4×10^{16} g s^{-1}. The recurrence time of the outbursts is approximately one year. The second outburst seen in this figure is enlarged in Fig. (3.10)

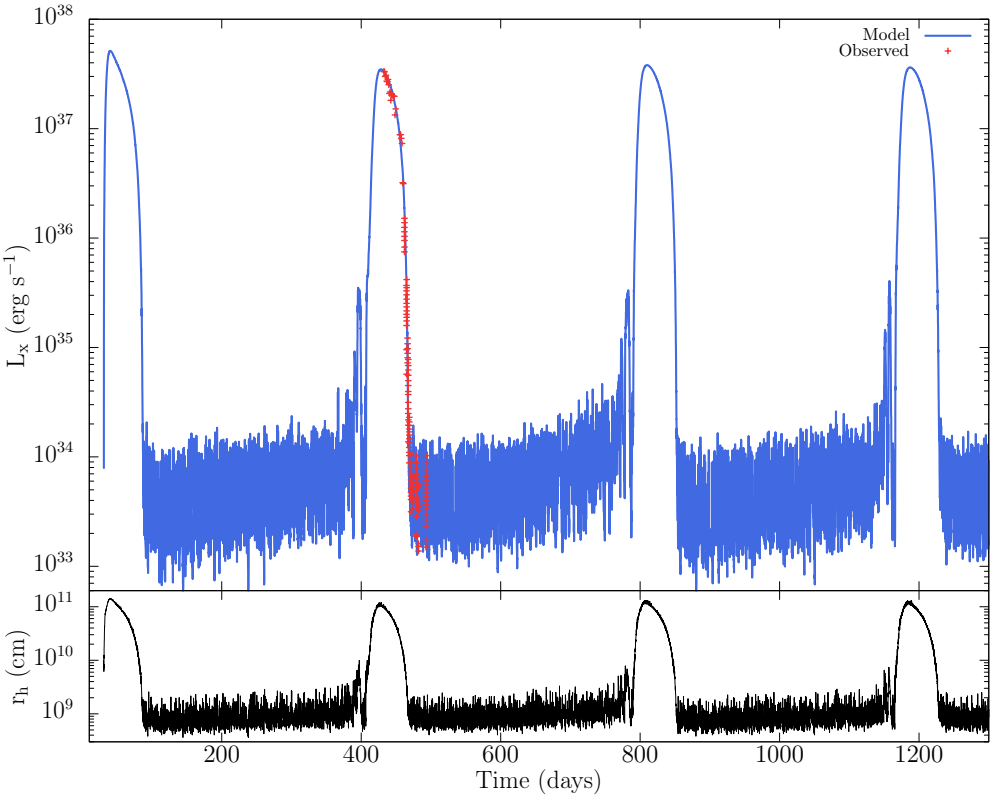

Figure 3.10 The second outburst seen in Fig. (3.9).

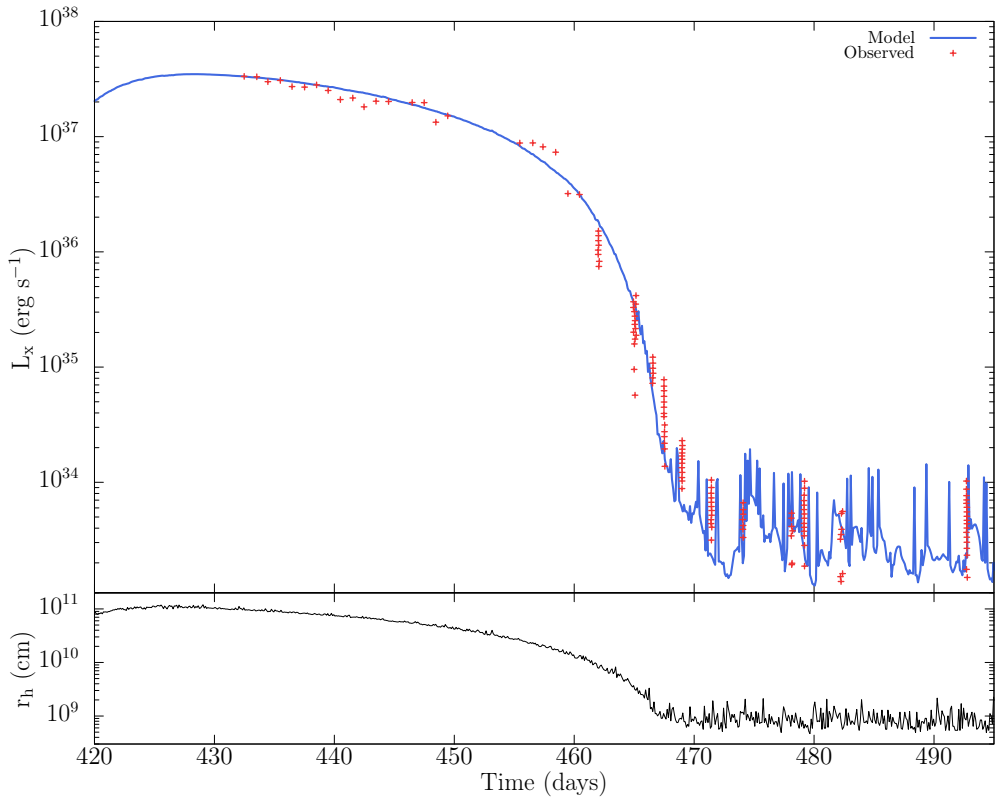

4. SUMMARY AND CONCLUSIONS

In this thesis, we have investigated the X-ray outburst light curve and the recurrence characteristics of a prototypical NSXT source Aql X-1. In most outbursts, X-ray outburst light curves of the source show some characteristic features. During the rise phase, the $L_{\rm X}$ peak reaches above $\sim 10^{37}$ erg s^{-1} within a few days. After the peak, $L_{\rm X}$ shows a slow exponential decay for a few weeks. Subsequently, $L_{\rm X}$ turns down rapidly forming a knee-like morphology when $L_{\rm X} \sim 10^{36}$ erg s^{-1}. Below this level, $L_{\rm X}$ decreases sharply to the quiescent state level $L_{\rm X} \sim 5 \times 10^{33}$ erg s^{-1}.

In general, for accreting magnetised stars, particularly for Aql X-1, it was suggested that the knee-like morphology followed by a sharp decay could be a sign of the onset of the propeller effect (Campana et al., 2014,1). In this work, we have tested whether the outburst light curve of the source can be modelled without invoking the propeller effect, investigating the physical reasons producing typical characteristics of the X-ray outburst light curves of the source in the frame of the DIM. We have also studied the recurrence characteristics of the source with the same model.

First, we have performed a parameter study to see the effects of the disc parameters, namely the kinematic viscosity parameter α, irradiation parameter C, and disc mass $M_{\rm disc}$ on the outburst light curve. With illustrative numerical simulations, we have obtained the following results: (i) For a given $M_{\rm disc}$, the details of initial mass distribution do not affect the decay properties of the $L_{\rm X}$ curve. (ii) The model curves obtained with different $M_{\rm disc}$ values show different $L_{\rm X}$ peaks and outburst fluences, but rather similar slopes below $L_{\rm X} \sim 10^{36}$ erg s^{-1}. (iii) With changing $\alpha_{\rm h}$, slopes of both initial and sharp decay curves change. Nevertheless, there is not a particular $\alpha_{\rm h}$ that can produce the $L_{\rm X}$ slopes in both decay phases in agreement with the observed X-ray outburst light curves of Aql X-1. (iv) The model outburst light curves are very similar with different $\alpha_{\rm c}$ parameters; that is, the exact value of $\alpha_{\rm c}$ does not have a significant effect on the outburst light curve. (v) Stronger $F_{\rm irr}$ with a constant C parameter produces X-ray outbursts with larger durations. However, the simulations with different C values produce $L_{\rm X}$ decays with similar slopes below $L_{\rm X} \sim 10^{36}$ erg s^{-1} that are not consistent with the observed sharper

decay curves of Aql X-1. (vi) $F_{\rm irr}$ calculated with the h/r ratio varying with $\dot{M}$ produces a sharper $L_{\rm X}$ decay phase consistently with the observed $L_{\rm X}$ curves of Aql X-1.

We have shown through these numerical calculations that the sharp decay observed in the X-ray outburst light curves of Aql X-1 below $L_{\rm X} \sim$ a few 10^{36} erg s^{-1} cannot be reproduced by only changing disc parameters without taking the h/r dependence of C into account. In simulation 7, including the local $\dot{M}$ dependence of h/r ratio in the C calculations, we have obtained model light curves similar to those of Aql X-1. Considering the results of our simulations summarised above, we have concentrated on the 2010 X-ray outburst data of Aql X-1. The data show sharp fluctuations during both the sharp decay phase and in the quiescent state. Without performing numerical fits, we have looked for the model curves that can reproduce seemingly good fits to the characteristic features of the observed X-ray light curve. Subsequently, we have investigated the model curves that can reproduce long-term recurrence properties of the source as well.

We have shown that the X-ray outburst light curve of Aql X-1 can be reproduced with DIM taking the $\dot{M}$ dependence of h/r into account in the calculations of the X-ray irradiation strength. In our model, the source of $L_{\rm X}$ is the accretion onto the star throughout the outburst state. In the model, we did not invoke the propeller effect or any partial accretion, which is proposed in earlier work to account for the knee and the following sharp decline in the $L_{\rm X}$ decay curve (Lipunova et al., 2022). The model is in agreement with the observed $L_{\rm X}$ in quiescence as well. In quiescence, observed $L_{\rm X}$ shows sharp fluctuations with up to ten-fold $L_{\rm X}$ variations (Bernardini et al., 2013; Coti Zelati et al., 2014). Similar $L_{\rm X}$ flares are also seen in our model curve. Nevertheless, it is not possible to model the details of these fluctuations due to the low radial resolution of the innermost disc in our model (see Ch. 3). These results imply that the source does not enter the propeller phase along the outburst state or in quiescence. This means that $r_{\rm in} \leq r_{\rm co}$ in the quiescent state with $\dot{M}_{\rm in} \sim 3 \times 10^{13}$ g s^{-1}. Together with strong propeller condition $r_\eta > 1.26 r_{\rm co}$ (see. Ertan 2021 for details), this gives an upper limit to the strength of the magnetic dipole field, which is $\sim 2.3 \times 10^8$ G on the surface of the star. Ongoing accretion during the quiescent state could also be the reason for the lack of radio pulsations from Aql X-1.

With the same model, we have also investigated the recurrence properties of the X-ray outbursts of Aql X-1. In the model, we represent the mass flow from the companion to the outer disc with a continuous mass addition into the radial grid at $r = r_{\rm circ}$ at each time step. The light curve seen in Fig. (3.9) is produced with

$\dot{M}_{\rm c} = 4 \times 10^{16}$ g s^{-1} and outbursts have a recurrence time of approximately one year. Interestingly, the second and fourth outbursts in the long-term model light curve can also reproduce the 2010 X-ray outburst light curve of Aql X-1 naturally (see Fig. 3.9 and 3.10), which is also very similar to the 1997 outburst light curve (Campana et al., 2014). The recurrence time of the outburst produced in the model is also in agreement with the observations of Aql X-1.

In future work, we will develop the model applied to Aql X-1 in this thesis to model the X-ray light curves of the transient accreting millisecond pulsars consistently with their measured rotational properties. For some of these sources, $\dot{P}$ measurements are available during the outburst states, while for others, $\dot{P}$ along the quiescent state is estimated from the P measurements during the successive outburst states. All these sources will be in the scope of our future work.

BIBLIOGRAPHY

Alexander, D. R. & Ferguson, J. W. (1994). Low-Temperature Rosseland Opacities. , *437*, 879.

Archibald, A. M., Stairs, I. H., Ransom, S. M., Kaspi, V. M., Kondratiev, V. I., Lorimer, D. R., McLaughlin, M. A., Boyles, J., Hessels, J. W., Lynch, R., et al. (2009). A radio pulsar/x-ray binary link. *Science*, *324*(5933), 1411–1414.

Baade, W. & Zwicky, F. (1934). Cosmic Rays from Super-novae. *Proceedings of the National Academy of Science*, *20*(5), 259–263.

Bassa, C., Patruno, A., Hessels, J., Keane, E., Monard, B., Mahony, E., Bogdanov, S., Corbel, S., Edwards, P., Archibald, A., et al. (2014). A state change in the low-mass x-ray binary xss j12270- 4859. *Monthly Notices of the Royal Astronomical Society*, *441*(2), 1825–1830.

Bernardini, F., Cackett, E. M., Brown, E. F., D'Angelo, C., Degenaar, N., Miller, J. M., Reynolds, M., & Wijnands, R. (2013). Daily multiwavelength Swift monitoring of the neutron star low-mass X-ray binary Cen X-4: evidence for accretion and reprocessing during quiescence. , *436*(3), 2465–2483.

Campana, S., Brivio, F., Degenaar, N., Mereghetti, S., Wijnands, R., D'Avanzo, P., Israel, G. L., & Stella, L. (2014). The return to quiescence of Aql X-1 following the 2010 outburst. *Monthly Notices of the Royal Astronomical Society*, *441*(3), 1984–1991.

Campana, S., Coti Zelati, F., & D'Avanzo, P. (2013). Mining the Aql X-1 long-term X-ray light curve. *Monthly Notices of the Royal Astronomical Society*, *432*(2), 1695–1700.

Campana, S., Stella, L., Mereghetti, S., & de Martino, D. (2018). A universal relation for the propeller mechanisms in magnetic rotating stars at different scales. , *610*, A46.

Coti Zelati, F., Campana, S., D'Avanzo, P., & Melandri, A. (2014). A year in the life of the low-mass X-ray transient Aql X-1. , *438*(3), 2634–2641.

Davidson, K. & Ostriker, J. P. (1973). Neutron-Star Accretion in a Stellar Wind: Model for a Pulsed X-Ray Source. , *179*, 585–598.

De Jong, J., Van Paradijs, J., & Augusteijn, T. (1996). Reprocessing of x rays in low-mass x-ray binaries. *Astronomy and Astrophysics*, *314*, 484–490.

Dubus, G., Hameury, J.-M., & Lasota, J.-P. (2001). The disc instability model for x-ray transients: Evidence for truncation and irradiation. *Astronomy & Astrophysics*, *373*(1), 251–271.

Dubus, G., Lasota, J.-P., Hameury, J.-M., & Charles, P. (1999). X-ray irradiation in low-mass binary systems. *Monthly Notices of the Royal Astronomical Society*, *303*(1), 139–147.

Ertan, Ü. (2017). The inner disc radius in the propeller phase and accretion-propeller transition of neutron stars. , *466*(1), 175–180.

Ertan, Ü. (2018). Accretion and propeller torque in the spin-down phase of neutron stars: The case of transitional millisecond pulsar psr j1023+ 0038. *Monthly Notices of the Royal Astronomical Society: Letters*, *479*(1), L12–L16.

Ertan, Ü. (2021). On the torque reversals of accreting neutron stars. *Monthly Notices*

of the Royal Astronomical Society, *500*(3), 2928–2936.

Ertan, U. & Alpar, M. A. (2002). On the outbursts of black hole soft x-ray transients. *A&A*, *393*(1), 205–214.

Frank, J., King, A., & Raine, D. J. (2002). *Accretion Power in Astrophysics: Third Edition*.

Galloway, D. K., Muno, M. P., Hartman, J. M., Psaltis, D., & Chakrabarty, D. (2008). Thermonuclear (Type I) X-Ray Bursts Observed by the Rossi X-Ray Timing Explorer. , *179*(2), 360–422.

Gencali, A. A., Niang, N., Toyran, O., Ertan, Ü., Ulubay, A., Şaşmaz, S., Devlen, E., Vahdat, A., Özcan, Ş., & Alpar, M. A. (2022). The torque reversals of 4u 1626–67. *Astronomy & Astrophysics*, *658*, A13.

Ghosh, P. & Lamb, F. K. (1979). Accretion by rotating magnetic neutron stars. III. Accretion torques and period changes in pulsating X-ray sources. , *234*, 296–316.

Gold, T. (1968). Rotating neutron stars as the origin of the pulsating radio sources. *Nature*, *218*, 731–732.

Hessels, J. W., Ransom, S. M., Stairs, I. H., Freire, P. C., Kaspi, V. M., & Camilo, F. (2006). A radio pulsar spinning at 716 hz. *Science*, *311*(5769), 1901–1904.

Hōshi, R. (1979). Accretion model for outbursts of dwarf nova. *Progress of Theoretical Physics*, *61*(5), 1307–1319.

Iglesias, C. A. & Rogers, F. J. (1996). Updated Opal Opacities. , *464*, 943.

Illarionov, A. F. & Sunyaev, R. A. (1975). Why the Number of Galactic X-ray Stars Is so Small? , *39*, 185.

King, A. (1998). Outbursts of irradiated accretion discs. *Monthly Notices of the Royal Astronomical Society*, *296*(4), L45–L50.

King, A. & Ritter, H. (1998). The light curves of soft x-ray transients. *Monthly Notices of the Royal Astronomical Society*, *293*(1), L42–L48.

Kluźniak, W. & Rappaport, S. (2007). Magnetically torqued thin accretion disks. *The Astrophysical Journal*, *671*(2), 1990.

Kretschmar, P., Fürst, F., Sidoli, L., Bozzo, E., Alfonso-Garzón, J., Bodaghee, A., Chaty, S., Chernyakova, M., Ferrigno, C., Manousakis, A., et al. (2019). Advances in understanding high-mass x-ray binaries with integraland future directions. *New Astronomy Reviews*, *86*, 101546.

Lamb, F. K., Pethick, C. J., & Pines, D. (1973). A Model for Compact X-Ray Sources: Accretion by Rotating Magnetic Stars. , *184*, 271–290.

Lasota, J.-P. (2001). The disc instability model of dwarf novae and low-mass X-ray binary transients. , *45*(7), 449–508.

Lipunova, G., Malanchev, K., Tsygankov, S., Shakura, N., Tavleev, A., & Kolesnikov, D. (2022). Physical modelling of viscous disc evolution around magnetized neutron star. Aql X-1 2013 outburst decay. , *510*(2), 1837–1856.

Liu, Q. Z., van Paradijs, J., & van den Heuvel, E. P. J. (2006). Catalogue of high-mass X-ray binaries in the Galaxy (4th edition). , *455*(3), 1165–1168.

Lovelace, R., Romanova, M., & Bisnovatyi-Kogan, G. (1995). Spin-up/spin-down of magnetized stars with accretion discs and outflows. *Monthly Notices of the Royal Astronomical Society*, *275*(2), 244–254.

Lovelace, R., Romanova, M., & Bisnovatyi-Kogan, G. (1999). Magnetic propeller outflows. *The Astrophysical Journal*, *514*(1), 368.

Manchester, R. N., Hobbs, G. B., Teoh, A., & Hobbs, M. (2005). The australia

telescope national facility pulsar catalogue. *The Astronomical Journal*, *129*(4), 1993.

Osaki, Y. (1974). An accretion model for the outbursts of u geminorum stars. *Publications of the Astronomical Society of Japan*, *26*, 429–436.

Papitto, A. & Martino, D. d. (2022). *Transitional Millisecond Pulsars*, (pp. 157–200). Cham: Springer International Publishing.

Psaltis, D. (2006). Accreting neutron stars and black holes: a decade of discoveries. In *Compact stellar X-ray sources*, volume 39 (pp. 1–38).

Sazonov, S., Paizis, A., Bazzano, A., Chelovekov, I., Khabibullin, I., Postnov, K., Mereminskiy, I., Fiocchi, M., Bélanger, G., Bird, A., Bozzo, E., Chenevez, J., Santo, M. D., Falanga, M., Farinelli, R., Ferrigno, C., Grebenev, S., Krivonos, R., Kuulkers, E., Lund, N., Sanchez-Fernandez, C., Tarana, A., Ubertini, P., & Wilms, J. (2020). The galactic lmxb population and the galactic centre region. *New Astronomy Reviews*, *88*, 101536.

Shakura, N. I. & Sunyaev, R. A. (1973). Black holes in binary systems. Observational appearance. , *24*, 337–355.

Smak, J. (1971). Eruptive binaries. *International Astronomical Union Colloquium*, *15*, 248–267.

Tan, C. M., Bassa, C. G., Cooper, S., Dijkema, T. J., Esposito, P., Hessels, J. W. T., Kondratiev, V. I., Kramer, M., Michilli, D., Sanidas, S., Shimwell, T. W., Stappers, B. W., van Leeuwen, J., Cognard, I., Grießmeier, J. M., Karastergiou, A., Keane, E. F., Sobey, C., & Weltevrede, P. (2018). LOFAR Discovery of a 23.5 s Radio Pulsar. , *866*(1), 54.

Ustyugova, G., Koldoba, A., Romanova, M., & Lovelace, R. (2006). "propeller" regime of disk accretion to rapidly rotating stars. *The Astrophysical Journal*, *646*(1), 304.

van Paradijs, J. (1996). On the Accretion Instability in Soft X-Ray Transients. , *464*, L139.